

Research on efficient active T-S wave generation method in boundary layer

Peifan Li¹, Zhen Cao¹, Dong Li¹

¹School of Aeronautics, Northwestern Polytechnical University, Xi'an, PR China

Abstract

The transition of the boundary layer is closely related to the flight of the aircraft. The laminar boundary layer is favored because of its low friction drag. In order to control the T-S instability, a set of T-S waves can be artificially excited in the boundary layer. Its phase is opposite to the phase of the T-S wave excited by the external disturbance, and the two are linearly superimposed, thereby reducing the amplitude of the total T-S wave and delaying the occurrence of the transition. In this paper, T-S waves excited by various disturbances are studied by Direct Numerical Simulation (DNS) and compared with Linear Stability Theory (LST). Some of the results are reproduced in wind tunnel experiments. The receptivity phenomenon of the laminar boundary layer over a zero-pressure-gradient flat plate is analyzed, and the results obtained by three research methods are in good agreement. Firstly, the characteristics of the T-S waves excited by single-period wall blowing and suction disturbances, referred to as the "elementary wave" (EW), are analyzed and organized. The amplitude of the EW does not conform to the Linear Stability Theory, and its frequency is not entirely equal to the disturbance frequency. Subsequently, the study finds that as the number of disturbance periods increases, the amplitude of the T-S waves at some streamwise locations exhibits a characteristic where the amplitudes at the beginning and end are greater than those in the middle. Then, six intermittent blowing and suction forms are proposed, and a quantitative comparison of these six blowing and suction control methods is carried out. Ultimately, an efficient method for generating T-S waves that can reduce the pump drag by more than 12% is proposed.

1. Introduction

In recent years, the situation of climate change has been serious, bringing unprecedented challenges and tests to human production and daily life. Amidst the quest for energy conservation and emission reduction, the notion of "green aviation" has emerged as a critical benchmark, presenting aircraft designers with a heightened set of requirements and intricate challenges. Innovative technologies aimed at reducing energy consumption and emissions—encompassing laminar flow control, electric propulsion as showcased in Figure 1, distributed propulsion systems, sustainable aviation fuel highlighted in Figure 2, and hydrogen-powered solutions—are increasingly taking center stage in the realm of applied research.



Figure 1 – NASA's X-57 Maxwell all electric aircraft [1]



Figure 2 – Sustainable Aviation Fuel (SAF) [2]

Frictional drag accounts for a significant proportion of the total drag in high-subsonic and transonic aircraft, and reducing frictional drag is of great importance for improving aircraft performance and achieving green aviation. Laminar frictional drag is much less than turbulent frictional drag, hence expanding the laminar flow area, or even achieving fully laminar flow, is an important way to reduce drag. The importance of hybrid laminar flow control (HLFC) technology is emphasized in the aircraft outlooks up to 2050 of IATA[3], DLR[4], ATI[5] and AIA[6].

AllCraft	Technolo	ду коас	тар со	2050
			5	

Group	Concept	EIS	TRL	Fuel Efficiency Benefits)
New Engine Architecture (Ultra- High Bypass Ratio:	Advance Turbofan [24]	2020	8	20% (Trent 700)
	Ultrafan [24]	2025	7	25% (Trent 700)
	GE9X [25]	2020	8	10% (GE90-115B)
UHBR)	Counter Rotating Fan [22]	after 2020	3	15 to 20%
	Ultra-High Bypass Ratio Engine [26]	2025	5	20 to 25% (5 to 10% re LEAP)
Advanced Engine Concepts	Zero Hub Fan [22]	2020	7	2 to 4%
	Adaptive/Active Flow Control [22]	after 2020	2	10 to 20%
Engine Cycle	Ubiquitous Composites (2nd Gen) [22]	after 2020	3	10 to 15%
	Natural Laminar Flow [27]	after 2020	8	5 to 10%
Aerodynamics	Hybrid Laminar Flow [28]	after 2020	7	10 to 15%
	Variable Camber with New Control Surfaces [22]	after 2020	5	5 to 10%
	Spiroid Wingtip [22]	after 2020	7	2 to 6%
Systems	Electric taxiing system with Auto Transformer Rectifier Unit [29]	2021	8	3%
	Fuel Cells [30]	2020	8	1 to 5%

Figure 3 – IATA Aircraft Technology Roadmap to 2050

In the low-disturbance environment such as high-altitude flight of aircraft, there are four common boundary layer instability, which are T-S instability, CF instability, Görtler instability and contact line instability [7]. For the surface of the aircraft flying at subsonic speed and small sweep angle, T-S instability mainly affects the boundary layer transition. The T-S instability is dominated by the Tollmien-Schlichting (T-S) waves generated and developed along the streamwise direction in the boundary layer. After the external disturbance is introduced into the boundary layer, it interacts in the flow nonparallel caused by the leading edge or roughness of the object, and the T-S wave is excited. This process is called the receptivity stage of boundary layer transition [8].

In a seminal study conducted in 1948, Schubauer and Skramstad [9] made the groundbreaking observation of Tollmien-Schlichting (T-S) waves within the boundary layer, utilizing the precision of a low-turbulence wind tunnel coupled with the sensitivity of a Constant Temperature Anemometer (CTA). Their work laid the foundation by affirming the reality of T-S instability. Morkovin [10] first referred to the process of external disturbance entering the boundary layer as receptivity and determined the initial conditions of the amplitude, frequency, and phase of the unstable waves. Rogler

and Reshotko [11] theoretically analyzed the response of the boundary layer to convective vortices for the first time. Goldstein [12] used the method of matched asymptotic expansions to study the generation of the T-S waves with free-stream disturbances imposed on a flat-plate boundary layer. And then he [13] found that a small but relatively sudden variation of surface geometry can nevertheless produce a strong coupling effect between an externally imposed acoustic disturbance and a spatially growing T-S waves.

Subsequently, based on the above, Crouch [14] and Choudhari and Streett [15] used the finite Reynolds number method to study the excitation of unstable T-S waves in the Blasius boundary layer with the effect of the acoustic disturbance, local wall inhaling, and roughness. Bertolotti [16] used the projectile stability equation (PSE) to study the T-S waves in the Blasius boundary layer with the interaction between two-dimensional and three-dimensional vortex disturbances and the local roughness on the wall surface. Zhang and Zhou [17] studied the T-S waves excited by vortex disturbance in free flow of a two-dimensional boundary layer on a flat plate with direct numerical simulation. The relationship between the amplitude of the generated T-S waves and the geometry of the localized bump was clarified. Deng [18] studied the acoustic receptivity of the hypersonic blunt leading edge boundary layer using DNS with a high-order accuracy weighted-compact-nonlinear scheme (WCNS), and the difference between the receptivity of the cold wall and the adiabatic wall of the hypersonic flat plate boundary layer were compared.

As the understanding of receptivity, T-S wave and transition gradually deepened, researchers began to study the control of T-S instability. Part of the idea is this, a set of T-S waves can be artificially excited in the boundary layer. Its phase is opposite to the phase of the T-S wave excited by the external disturbance, and the two are linearly superimposed, thereby reducing the amplitude of the total T-S wave and delaying the occurrence of the transition. Robert [19] conducted an experiment which T-S wave in the boundary layer on a flat plate with zero pressure gradient were shown to be nearly canceled by interference with a second wave, 180° out-of-phase with the original disturbance. Li and Gaster [20] studied the active control of spatially evolving three-dimensional instability waves in the boundary layer. They used sensors to detect the on-coming disturbances and sent appropriate control signals to the downstream actuators to generate counteracting disturbances. The amplitudes of the disturbances downstream were significantly suppressed when the causal transfer function was applied. Sasaki and Morra [21] numerically studied the feedforward active control of T-S waves over incompressible 2D and 3D boundary layers. They found that the optimal linear-quadratic-Gaussian (LQG) controller leads to a similar control law and presents a comparable performance to the simpler, wave-cancellation scheme, indicating that the former acts via a destructive interference of the incoming wavepacket downstream of actuation. Simon, Markus and Tropea et al. [22] studied the control mechanism in the direct vicinity of the actuator using particle image velocimetry. They use of two cameras that allows measurement of two full wavelengths of the Tollmien-Schlichting waves and a detailed analysis of the cancellation process. Brennan, Gajjar and Hewitt [23] considered a localised (unsteady) wall heating/cooling to cancel the T-S wave. The nonlinear receptivity problem based on triple-deck scales is formulated and the linearised version solved both analytically as well as numerically. They found the wall heating/cooling function can be chosen such that there is no pressure response to the disturbance, meaning there is no generation of extra T–S waves.

Despite extensive research into the active control of T-S waves, practical implementation remains elusive. A primary obstacle hindering its progression into hybrid laminar flow control (HLFC) technology for real-world engineering applications is the substantial energy demands of the blowing and suction processes. This energy-intensive requirement engenders significant pump drag, translating into elevated control expenditures [24][25].

This study delves into the excitation of Tollmien-Schlichting (T-S) waves under the influence of diverse disturbances, employing Direct Numerical Simulation (DNS) for in-depth analysis and corroborating findings with Linear Stability Theory (LST). Key outcomes of this investigation are further substantiated through wind tunnel experiments, reinforcing the theoretical underpinnings with

empirical evidence. The study meticulously examines the receptivity phenomenon within the laminar boundary layer of a flat plate subjected to a zero-pressure-gradient environment. The convergence of results across three distinct research methodologies attests to their collective veracity and enhances the study's methodological robustness.

Initially, the study focuses on the intrinsic attributes of T-S waves excited by single-cycle wall blowing and suction disturbances, hereby denoted as "elementary waves" (EW). A meticulous analysis and systematic organization of these characteristics pave the way for a deeper comprehension of the underlying mechanisms. Further investigation reveals a notable trend with the escalation in the cycles of disturbances: at select streamwise locations, the T-S wave amplitudes manifest a peculiar pattern, highlighting increased amplitudes in the leading and trailing segments in comparison to the central portion. Subsequently, the study introduces six innovative intermittent blowing and suction methodologies, conducting an exhaustive quantitative comparison among these approaches, thereby elucidating their relative efficacies in the context of control methods. Ultimately, the study introduces an efficacious methodology for the generation of T-S waves, demonstrating its potential to significantly diminish pump drag by over 12%, offering a substantial advancement in flow control efficiency.

2. Numerical approach and Experiments configurations

2.1 Governing equations and numerical methods

The direct numerical simulation (DNS) method is used to solve the incompressible Navier-Stokes (NS) equation. The specific form of the equation is defined as

$$\begin{cases} \nabla u = 0\\ \frac{\partial u}{\partial t} + u \nabla u = -\frac{1}{\rho} \nabla p + v \Delta u \end{cases} \tag{1}$$

where u represents the velocity, t is time, ρ specifies the fluid density, p characterizes the pressure, v denotes the kinematic viscosity coefficient.

By non-dimensionalizing the equation

$$\begin{cases} x^* = \frac{x}{L} \\ u^* = \frac{u}{U} \\ t^* = \frac{tU}{L} \\ p^* = \frac{p}{\rho U^2} \\ Re = \frac{UL}{U} \end{cases}$$
 (2)

where L=1, $U=U_{\infty}$, we obtain a non-dimensional form of the two-dimensional incompressible N-S equation given by

$$\begin{cases} \nabla u^* = 0\\ \frac{\partial u^*}{\partial t^*} + u^* \nabla u^* = \nabla p^* + \frac{1}{Re} \Delta u^* \end{cases}$$
 (3)

The above incompressible N-S equation is solved based on the platform NEK5000 [26] by using the in-house modified code, which is basically based on the spectral element method (SEM) to provide geometrical flexibility, spectral accuracy and efficient parallelization.

2.2 Computational domain and grids

The computational geometry is a flat plate with the laminar boundary layer condition with a zero-flow direction pressure gradient, and the computational domain is sketched in Figure 1. The inlet of the domain is defined as x = -5, the plate is placed horizontally ($0 \le x \le 200$, y = 0), and the outlet is positioned at the right end of the plate. Overall, 276 nodes are arranged along the flow direction, and 33 nodes are arranged in the wall-normal direction, for a total of 9,108 nodes and 446,292 degrees of freedom. The spacing is exponentially distributed both in the wall-normal direction and the flow

direction of the flat plate section. The spacing is exponentially distributed with horizontal and vertical respectively. At the thickest area of the boundary layer, $y^+ < 0.5$.

The time integration is a second-order scheme. The time step Δt is chosen as 0.0002. The non-dimensional kinematic viscosity v is given as 0.0004, the non-dimensional density ρ is 1, and the criterion for pressure convergence residuals ε_p and velocity convergence residuals ε_v are both defined as 10^{-7} .

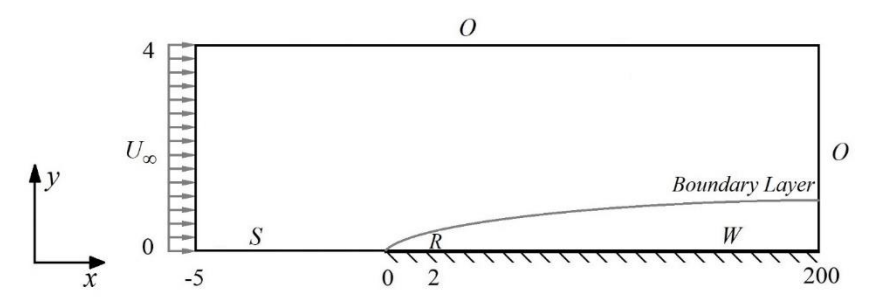


Figure 4 – The computational domain

The computational domain and boundary conditions are shown in Figure 4. When calculating the basic flow, there is no inhalation at the plate wall. When calculating the disturbed flow, the inhalation source (R) is placed at $2.097 \le x_{inhalation} \le 2.30$, where the disturbance velocity along the wall normal direction is defined as v_d . In Figure 4, "W" means non-slip boundary condition, "O" means the non-stress outflow boundary condition with no stress at any directions, "S" means the symmetric boundary condition, and "D" means the boundary condition, where the velocity along flow direction and the wall normal direction are defined as u_d and v_d , respectively.

2.3 Wind tunnel and equipment

The experiment was carried out in the Low Turbulence Wind Tunnel (LTW) at Northwestern Polytechnical University.

The LTW was built in 1989 and refreshed in 2010. The binary test section of the wind tunnel is a rectangle with a cross section of 0.4×1 meter and a length of 2.6 meters. The turbulence intensity is less than 0.02%.

The flat plate model was polished to 0.8µm rms fitted with a 20:1 MSE leading edge [27]. The flat plate was fixed to the wind tunnel and its trailing edge was fitted with a flap to control the flow pressure gradient. The flat plate is 2200 mm long, 395 mm wide and 10 mm thick, with a roughness element of 180µm thickness and 20 mm width. Acoustic disturbances were introduced by two HiVi E6.5 loudspeakers with a diameter of 164 mm and a total power of 240 Watts.

Velocity measurements were made by Dantec StreamLine Pro Constant Temperature Anemometer (CTA) with a 55P15 boundary layer type probe. The hot wire probes were mounted on a high-precision 3D traverse system.

The schematic of the experimental apparatus is given in Figure 5. The picture of the probe and the flat plate in the experiment is shown in Figure 6. The flow speed was 10m/s and the disturbance frequency was 80Hz. The measured T-S wave amplitudes were compared with linear stability theory and the results are shown in Figure 12. The good match verified the accuracy of the present experiment, so its result was used to make a quantitative comparison with the DNS result under a similar condition in Section 3.2.

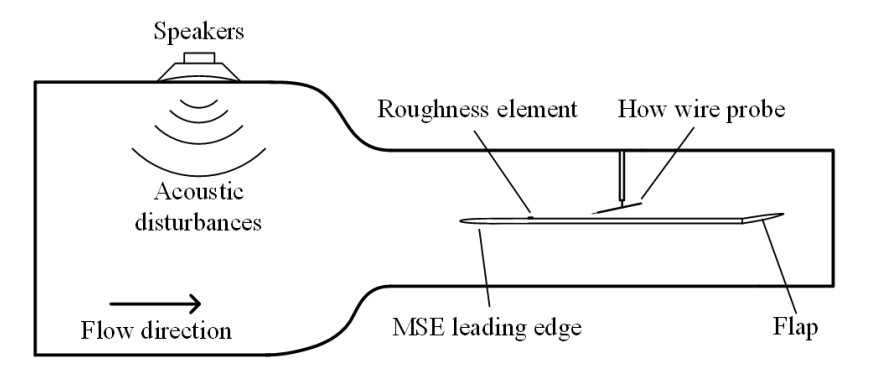


Figure 5 – Experimental set-up

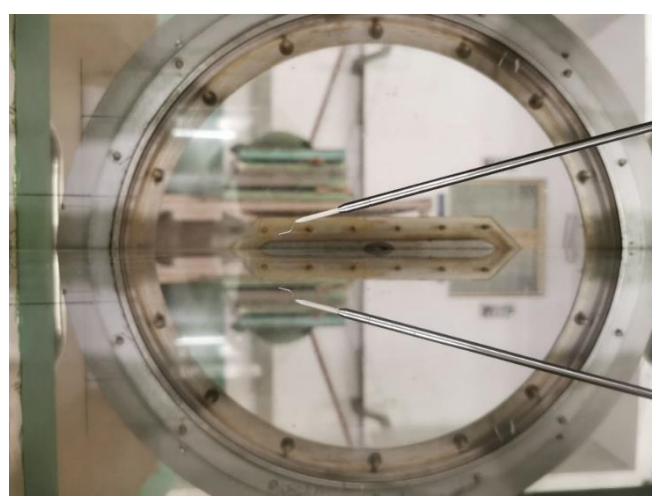


Figure 6 – Flat plate and the Dantec 55P15 boundary layer type probe. Notice the mirror-like appearance of the flat plate.

3. Validation of fundamental flow

3.1 Basic flow pressure gradient and velocity

Firstly, a steady-state solution of the fully converged flow field needs to be calculated before the disturbances are introduced, and this steady-state solution is used as an initial condition for solving the flow with the disturbances involved. In DNS, we choose $U_{\infty}=2$. In experiments, we choose $U_{\infty}=7$.

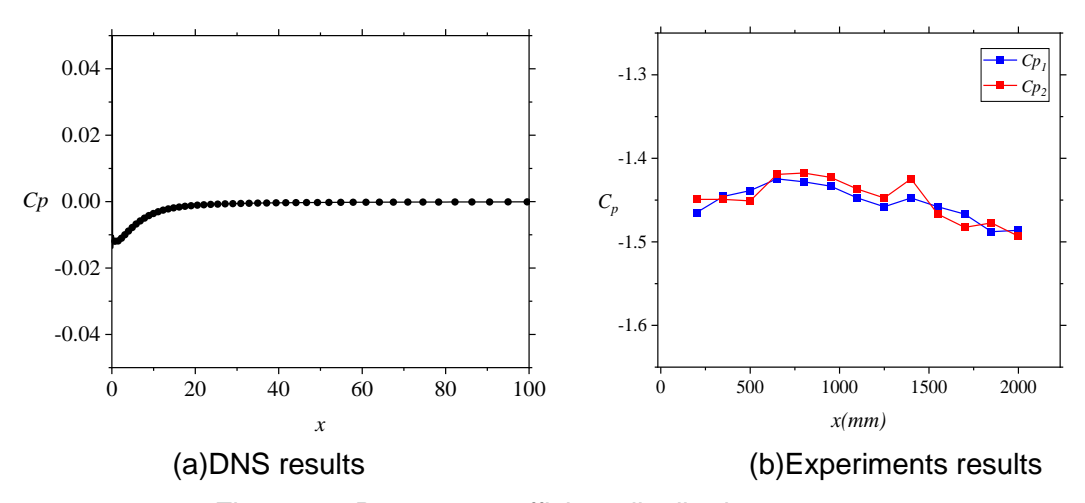


Figure 7 – Pressure coefficient distribution C_P .

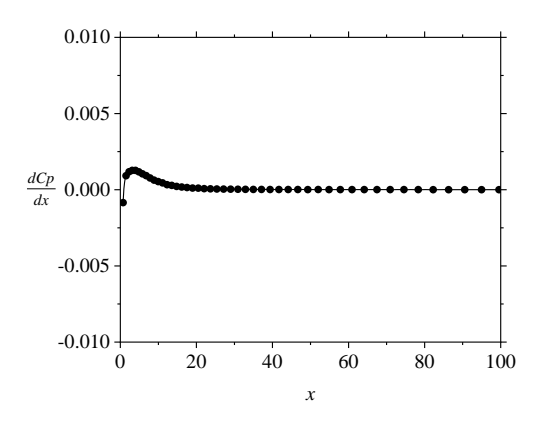


Figure 8 – The streamwise gradient $\frac{dCp}{dx}$ distribution obtained by the DNS

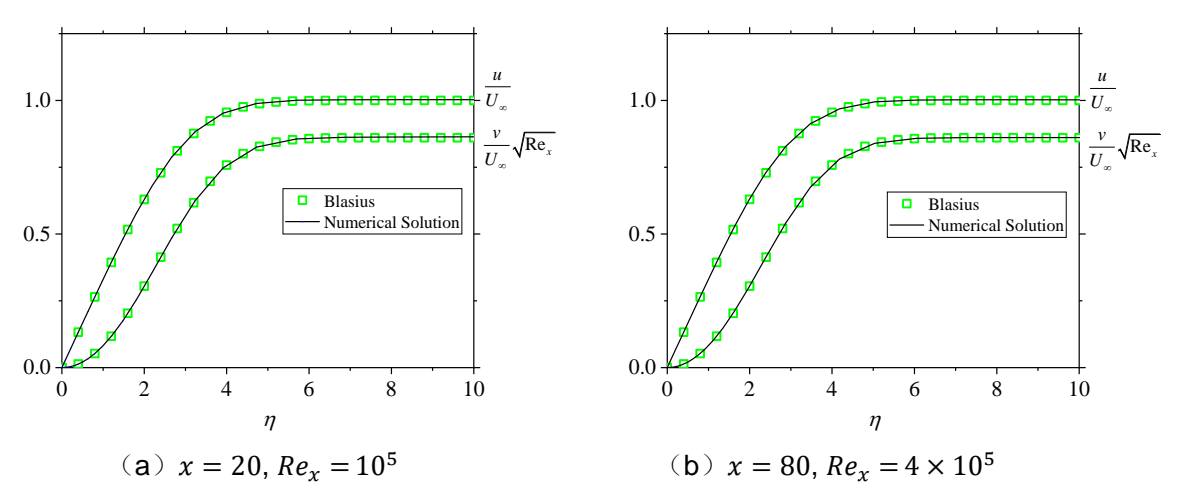


Figure 9 – streamwise and wall-normal velocity profiles obtained by the DNS

The streamwise pressure coefficient and the distribution of the pressure gradient of the basic flow are shown in Figure 7&8. The interference at the leading edge causes the pressure gradient to be slightly greater than zero in the area where x < 20, but it quickly recovers to a zero pressure gradient downstream. Figure 8 shows that the distribution of the streamwise and wall-normal velocity profiles, which well matched the Blasius solution. This all indicates that the numerical calculation results match well with the theoretical solution, demonstrating that the settings of the basic flow are well established and reliable, providing an ideal basic flow for the subsequent calculations.

3.2 LST DNS and experiments analysis

Before conducting the receptivity research, the appropriate laminar boundary layer basic flow has been obtained in Section 3.1. This section will introduce appropriate constant frequency external disturbances into the boundary layer and analyze the excited T-S waves.

In the DNS research case, the inhalation source (described in Section 2.2) is placed at the surface of the plate to apply the disturbance in the form of

$$\begin{cases} u_d = 0 \\ v_d = A_{disturb} \sin(\omega t) \end{cases}, 2.097 \le x \le 2.30, y = 0$$
 (4)

The dimensionless frequency is defined as follows

$$F = \frac{\omega v}{U_x^2} \times 10^6 \tag{5}$$

When selecting the amplitude of the disturbance $A_{disturb}$, careful consideration is necessary. It is important to ensure that $A_{disturb}$ is not so large as to cause bypass transition, nor so small

that it gets dissipated. After analysis and experimentation, $A_{disturb}$ is finally chosen to be 0.001. Figure 10 shows the streamwise velocity fluctuation (black line) of the T-S waves within the boundary layer at four different frequencies and their envelope lines (red line). Starting from the inhalation source, the velocity fluctuation values first increase sharply, then gradually decrease, then gradually increase again, and finally decrease to zero. The points where the amplitude changes from decreasing to increasing for the second time and from increasing to decreasing for the second time are called neutral points, which correspond to the first branch and the second branch of the neutral stability curve, respectively. It can also be observed that the wavelength of the T-S waves remains essentially constant in the streamwise direction.

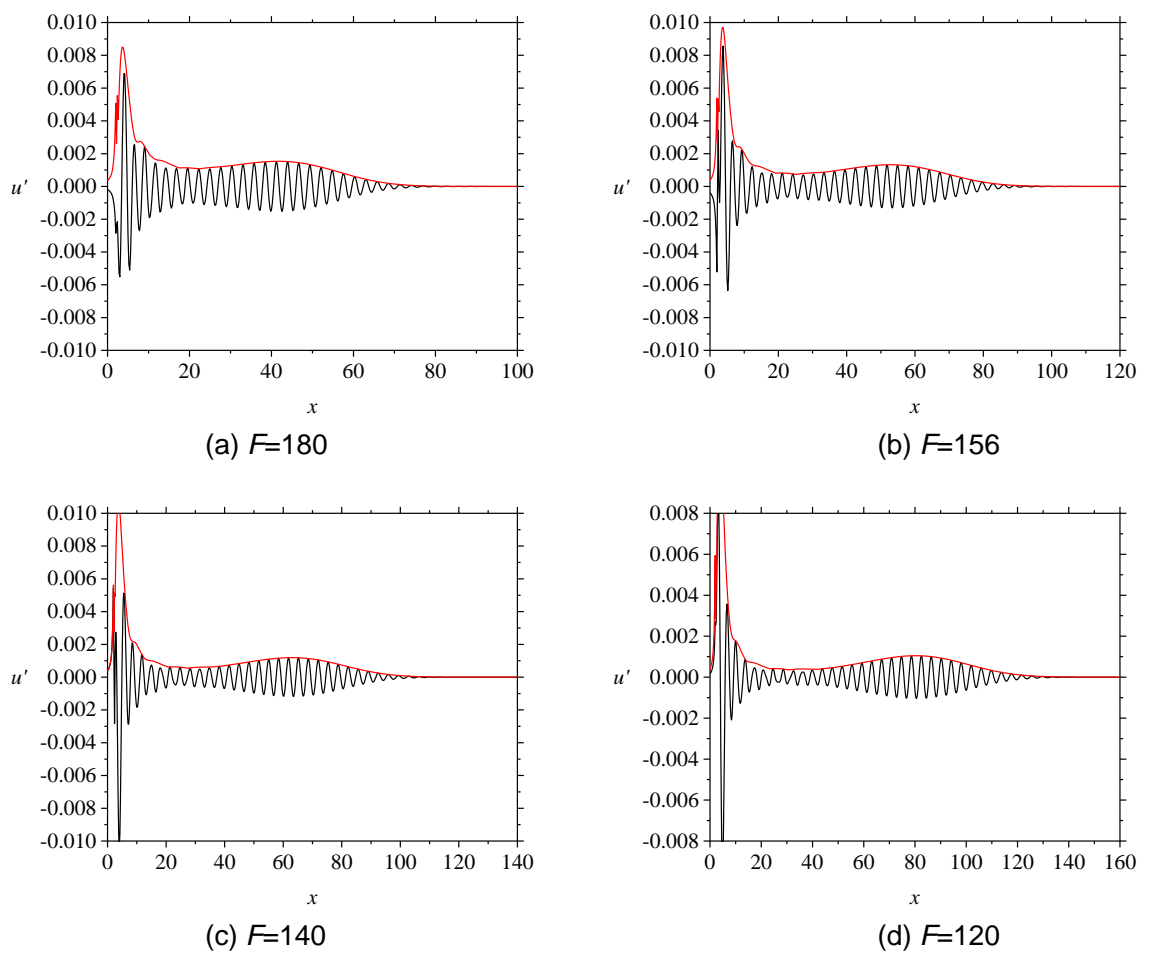


Figure 10 – Distribution of streamwise velocity fluctuation along y=0.095 obtained by the DNS

The neutral points are plotted on the neutral stability curve, resulting in Figure 11. The DNS results match well with the LST. The experimental results are influenced by the pressure gradient on the flat plate, with their neutral points being closer to the interior of the neutral curve.

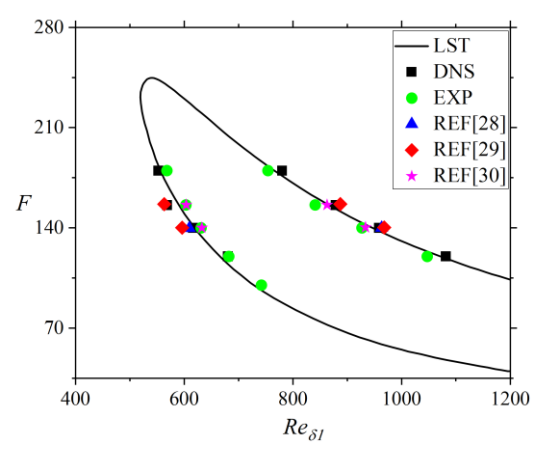


Figure 11 – Comparison of neutral points obtained from DNS experiments and linear stability theory

Further, the normal distribution of the T-S wave amplitude can be compared with the Linear Stability Theory (LST), with the results shown in Figure 12. The agreement between DNS, experimental data, and LST is good. This indicates that the DNS model, mesh, parameters, and other settings are well configured and can be further used to study the receptivity phenomena and T-S waves.

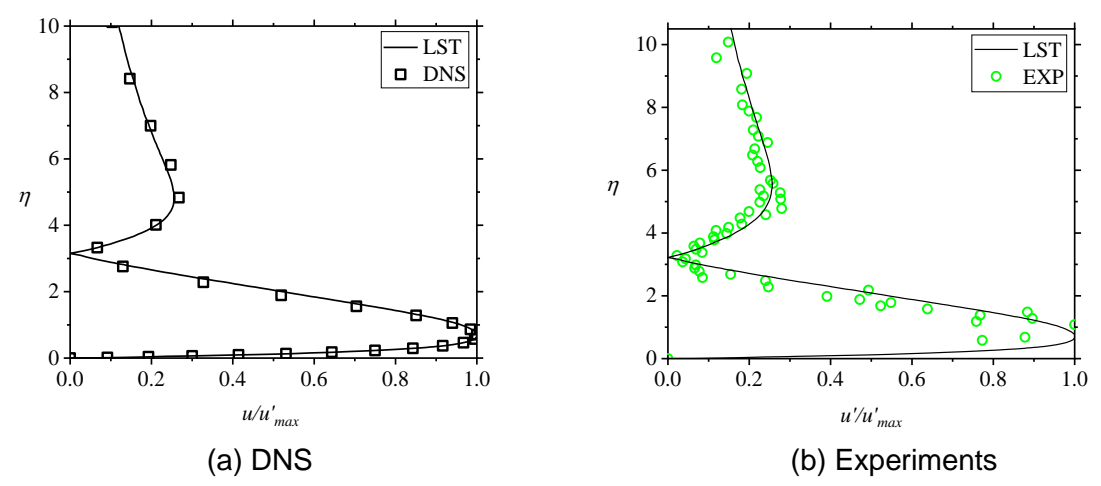
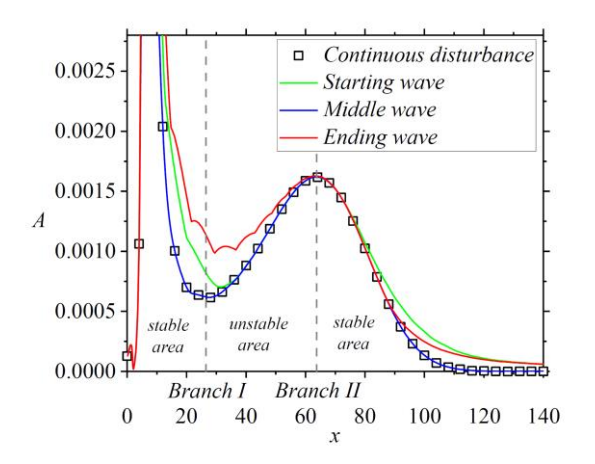


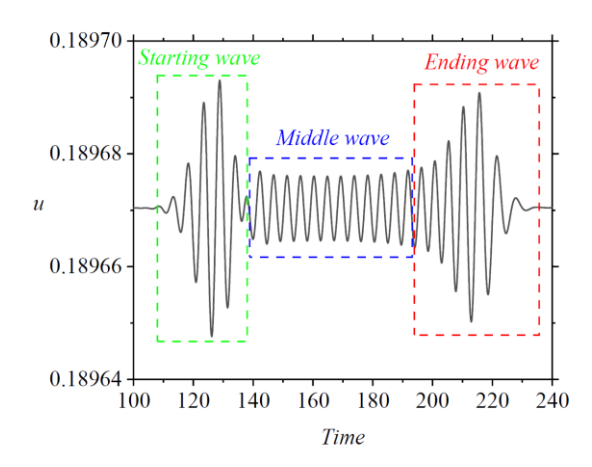
Figure 12 – Distribution of the T-S wave amplitude compare to LST

3.3 Starting, middle and ending wave

In previous studies, the authors found that the characteristics of T-S waves excited by finite periodic disturbances are quite different from T-S waves excited by continuous disturbances (CDTS).

Taking a set of T-S waves excited by a 20-cycle sinusoidal disturbance as an example (Figure 13). The T-S waves have three phases with different characteristics, temporally categorized as the starting, middle and ending wave. Along the flow direction, the middle wave continuously transforms into the starting wave and the ending wave. Downstream of the second branch of the neutral curve, the middle wave decays significantly faster than the starting and ending wave.





(a)Amplitudes along y=0.041

(b) Time traces of streamwise velocity at stable area

Figure 13 – Comparison of the amplitudes of the starting wave, middle wave, ending wave and T-S wave excited by a continuous disturbance

Figure 14 illustrates the moments at which the velocity fluctuations are zero at different streamwise positions along y=0.041 when F=140. The blue box in the figure represents external disturbances, with a wave speed equal to the free-stream velocity, which is 2, and the wavelength remains constant. Because the external disturbances entering this height are 2 to 3 orders of magnitude smaller than the T-S wave amplitude, the input disturbance part in the figure is overshadowed by the subsequent starting, middle and ending wave. The upper left green box in the figure represents the starting wave, the blue box represents the middle wave, and the red box represents the ending wave. From the most upstream to the most downstream, the frequency of the starting wave and ending wave gradually decreases, while the frequency of the middle wave remains constant.

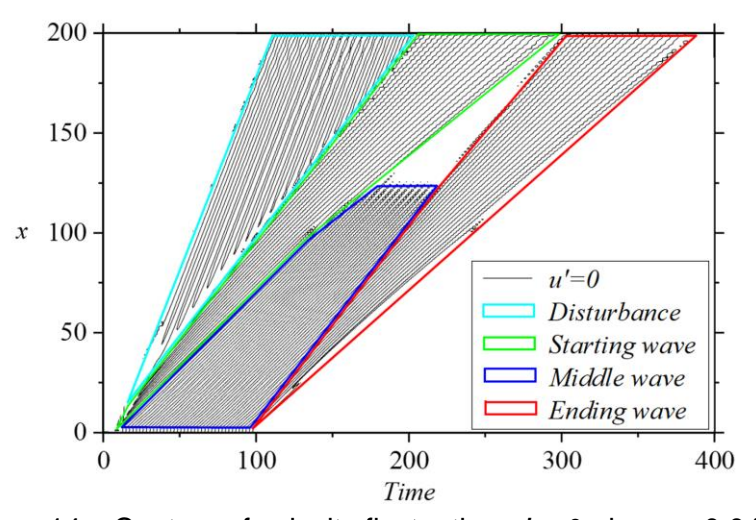


Figure 14 – Contour of velocity fluctuation u' = 0 along y=0.041

3.4 Elementary waves

To further investigate the causes of the generation of the starting, middle and ending waves, a single cycle disturbance is introduced into the flow field. Selecting $_{F=140}$ with the same disturbance amplitude as used in Section 3.2.

$$\begin{cases} v_R = 0.0 \le time < 10 \\ v_R = 0.01 \sin[1.40(time - 10)], 10 \le time \le 10 + \frac{2\pi}{1.4} \\ v_R = 0.10 + \frac{2\pi}{1.4} < time \le 400 \end{cases}$$
 (6)

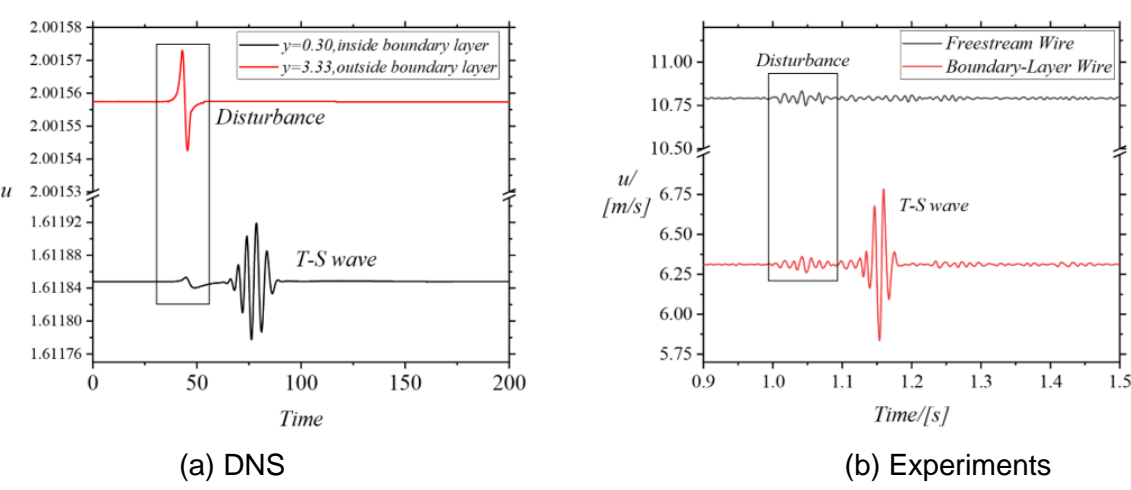


Figure 15 – Time traces of velocity obtained by DNS and experiment

Figure 15 shows the results of the calculations in this section at x=60.5 and the results of the wind tunnel experiments. Both the DNS and the experimental results show that the external disturbance propagates simultaneously inside and outside of the boundary layer and with essentially the same wave speed. Besides, DNS demonstrates some different results from the experiments, which are limited by the experimental conditions, and the amplitude of the external disturbance is not stable due to the complex reflection of sound waves in the wind tunnel.

For convenience, the T-S waves excited by a single-period disturbance are defined as the elementary wave and used in the rest of the paper.

The spatial distribution of the streamwise velocity fluctuation of elementary wave is shown in Figure 16. The phase transition mechanism of T-S waves can be clearly observed in the figure 16(a). However, it is quite important to note that the frequency of the elementary wave quickly undergoes a decrease with time, which is contrary to the characteristics of the CDTS.

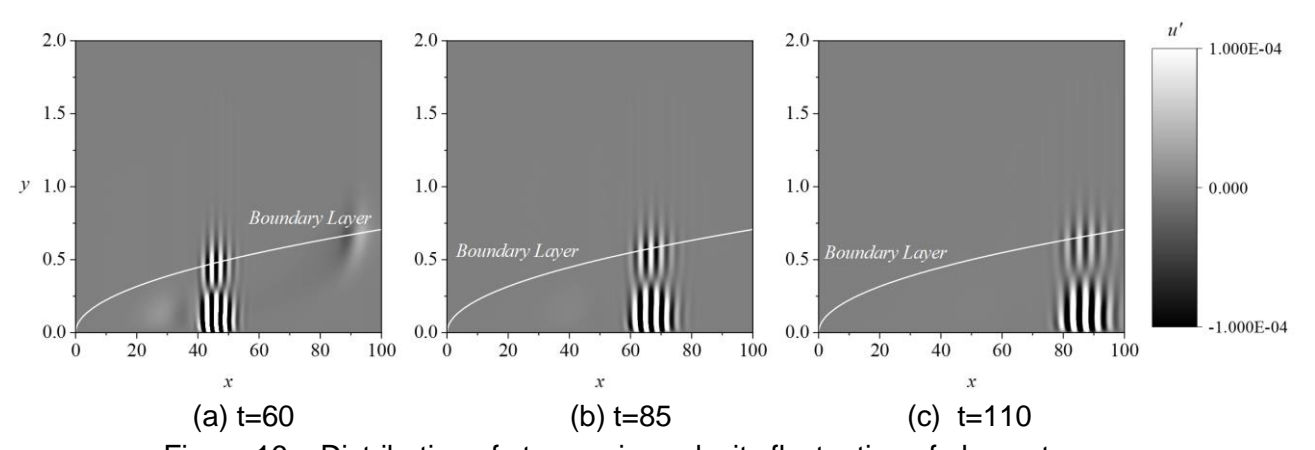


Figure 16 – Distribution of streamwise velocity fluctuation of elementary wave

4. New results

4.1 Analysis of the elementary wave

Depicted as in Figure 14, the velocity fluctuation diagram of the elementary wave, is shown in Figure 17(a). The frequency and wave speed characteristics of the elementary waves are basically the same as those of starting and ending waves. During the propagation process, the frequency of the elementary wave significantly decreases (as shown in Figure 17(b)). In the uppermost part of the flow, the elementary wave frequency is about 2.5 times of the input disturbance frequency. The elementary wave frequency decreases along the flow direction. Near the second branch of the neutral curve, the elementary wave frequency is 140, which is consistent with the frequency of the external disturbance.

The wave speed of elementary wave is roughly one-third of the incoming flow speed, but it also gradually decreases in the flow direction.

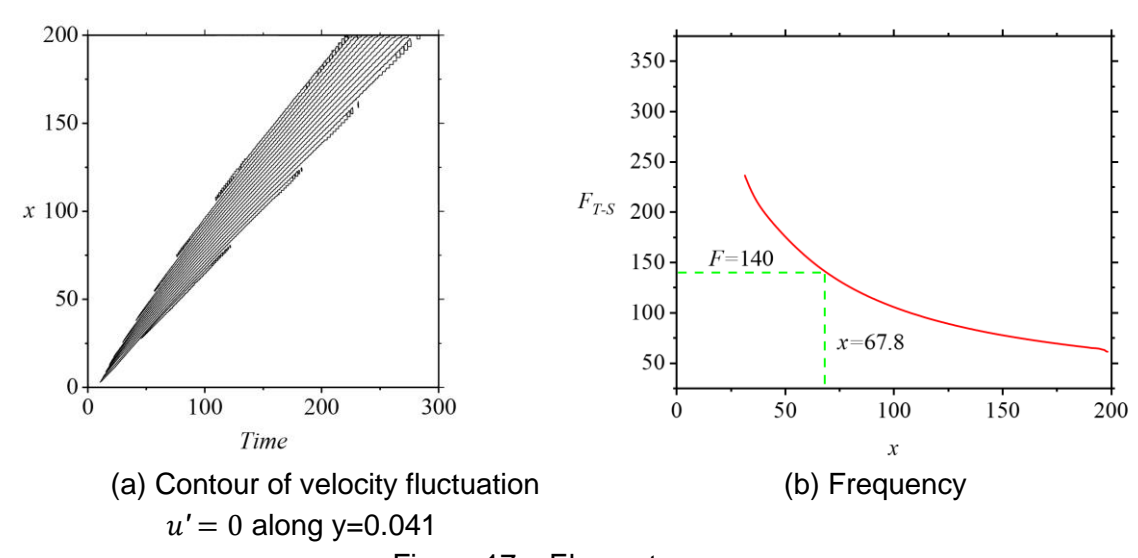


Figure 17 – Elementary wave

Further research indicates that if the elementary wave is superimposed according to the period of the external disturbance, the T-S wave excited by finite periodic disturbances is obtained. Considering that the amplitude of the starting and ending waves excited by finite periodic disturbances is significantly greater than the CDTS (as shown in Figure 13), it is considered to improve the efficiency of T-S wave generation by taking advantage of this. The aim is to reduce the pump drag generated during the HLFC process.

4.2 Intermittent blowing and suction

To fully exploit the properties of the elementary wave and to stimulate the starting and ending waves with significant amplitudes as much as possible, a method of intermittent blowing and suction is proposed to efficiently excite T-S waves. This approach leverages the characteristics of the elementary wave to enhance the efficiency of T-S wave generation.

Six methods of intermittent blowing and suction methods:

- 1. complete blowing + intermittent;
- 2. complete suction + intermittent;
- 3. complete cycle blowing and suction + intermittent;
- 4. complete blowing + intermittent + complete suction + intermittent
- 5. half cycle blowing + intermittent + half cycle blowing + intermittent + half cycle suction+ intermittent
- + half cycle blowing + intermittent + half cycle suction + intermittent;
- 6. half cycle blowing + intermittent + half cycle suction + intermittent + half cycle blowing+ intermittent
- + intermittent + half cycle suction + intermittent;

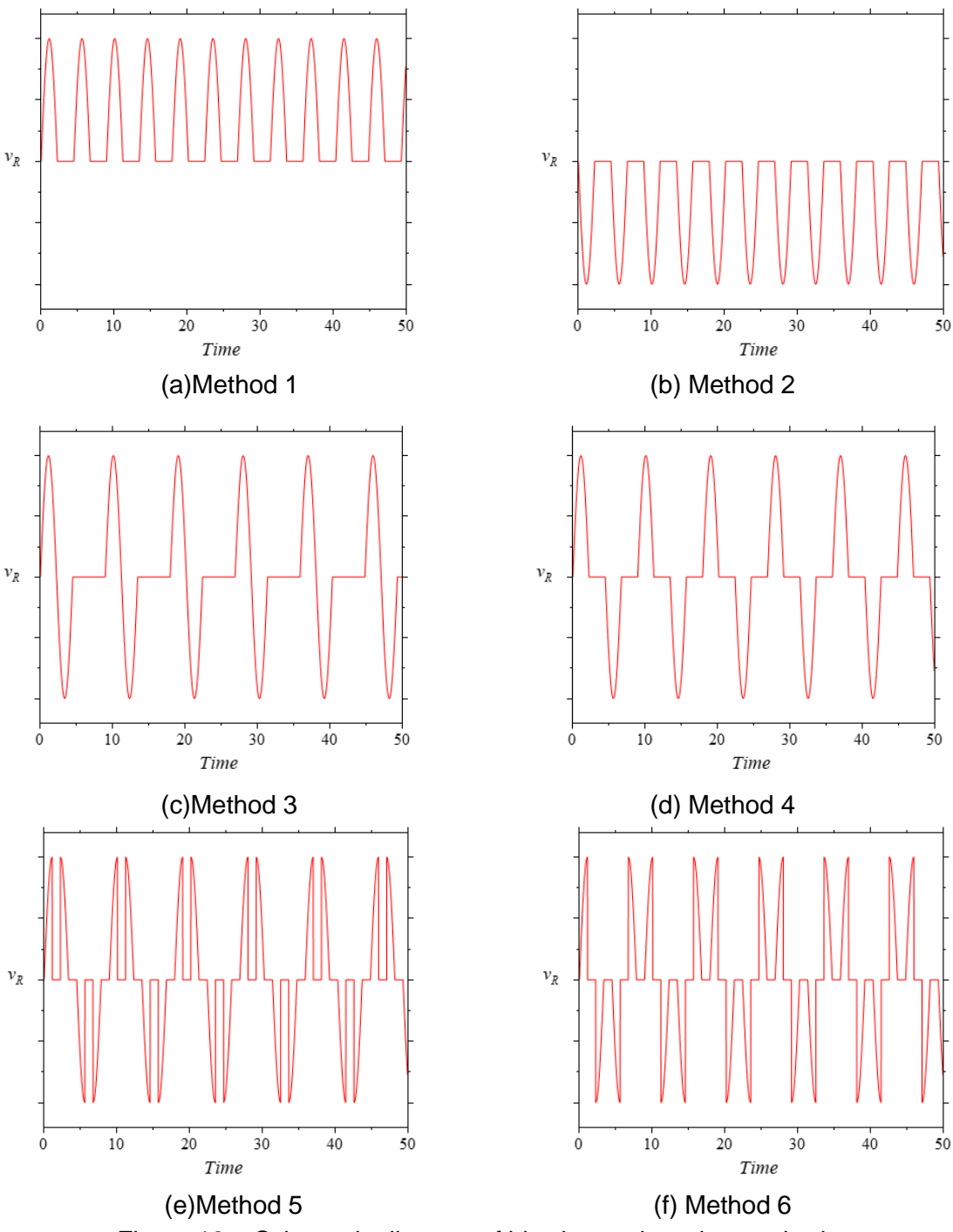


Figure 18 – Schematic diagram of blowing and suction methods

The first two blowing and suction methods alter the mass flow within the boundary layer, resulting in frequency characteristics that are markedly different from the last four methods. Consequently, the T-S waves excited by these methods exhibit unique characteristics. Moreover, since this approach does not involve zero-mass jet, these two methods do not possess the potential to control the T-S waves within the boundary layer.

Under the same blowing-suction frequency and duty ratio (DR), the maximum amplitude points of T-S waves generated by the latter four intermittent blowing-suction methods have the same flow direction. The duty ratio is defined as

$$DR = \frac{T_{V_R \neq 0}}{T_{V_R = 0} + T_{V_R \neq 0}} \tag{7}$$

where $T_{V_R \neq 0}$ is the length of time that the blowing-suction speed is not zero, $T_{V_R = 0}$ is the length of time that the blowing-suction speed is zero. The duty ratio in Figure 18 is 0.5.

4.3 Comparison of blowing and suction method

The spectral analysis of the four intermittent blowing-suction disturbance methods is shown in Figure 19. The fundamental frequency chosen is F=140. All four forms exhibit a sharp peak at the frequency F*DR, where Method 4 has the highest amplitude.

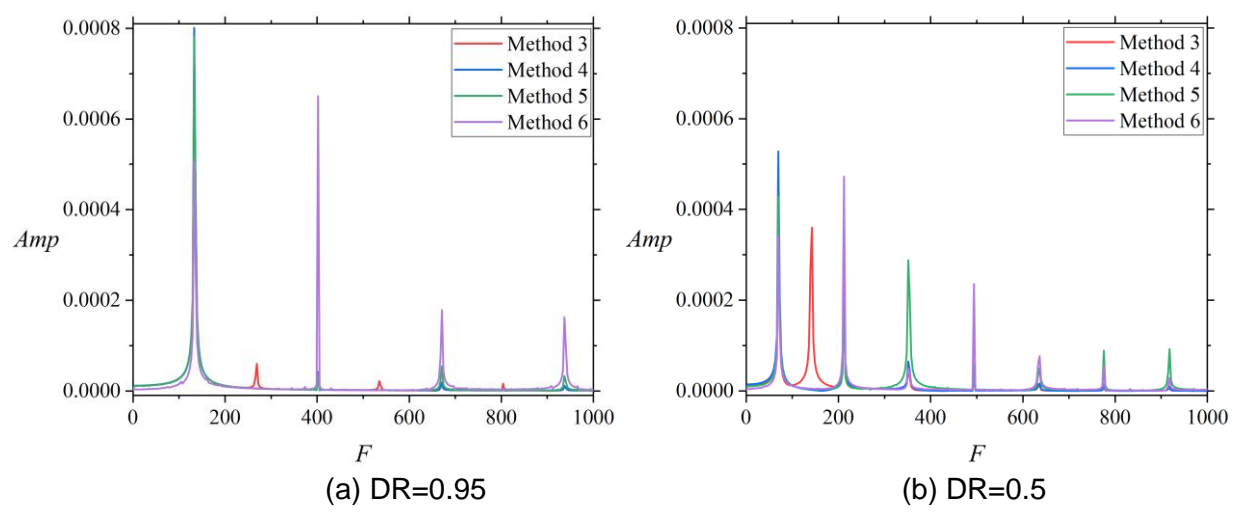


Figure 19 – Spectrum diagram of six methods (F=140)

Moreover, the efficiency of exciting T-S waves using the third to sixth blowing and suction methods is compared. Four types of disturbance inputs with F=140 and DR=0.95 are selected to be introduced into the boundary layer. The excited T-S waves are then studied and compared with the CDTS with F=133 (0.95*140). Figure 20 illustrates the amplitudes of the five scenarios near the second branch of the neutral stability curve. It is evident that the amplitude of the CDTS is the greatest, followed by the T-S waves excited by methods 4, 3, and 5, respectively. The smallest amplitude is that of the T-S waves excited by method 6.

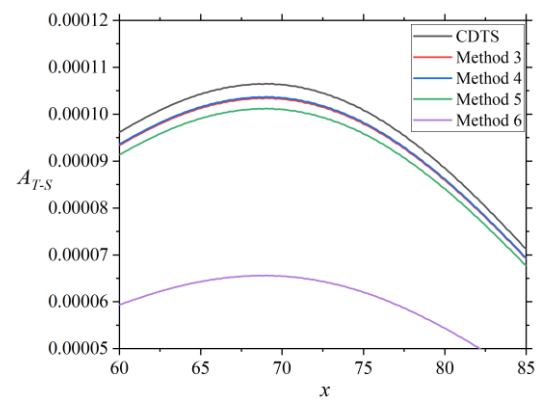


Figure 20 – Comparison of T-S wave amplitudes excited by four methods and CDTS near the second branch of the neutral curve

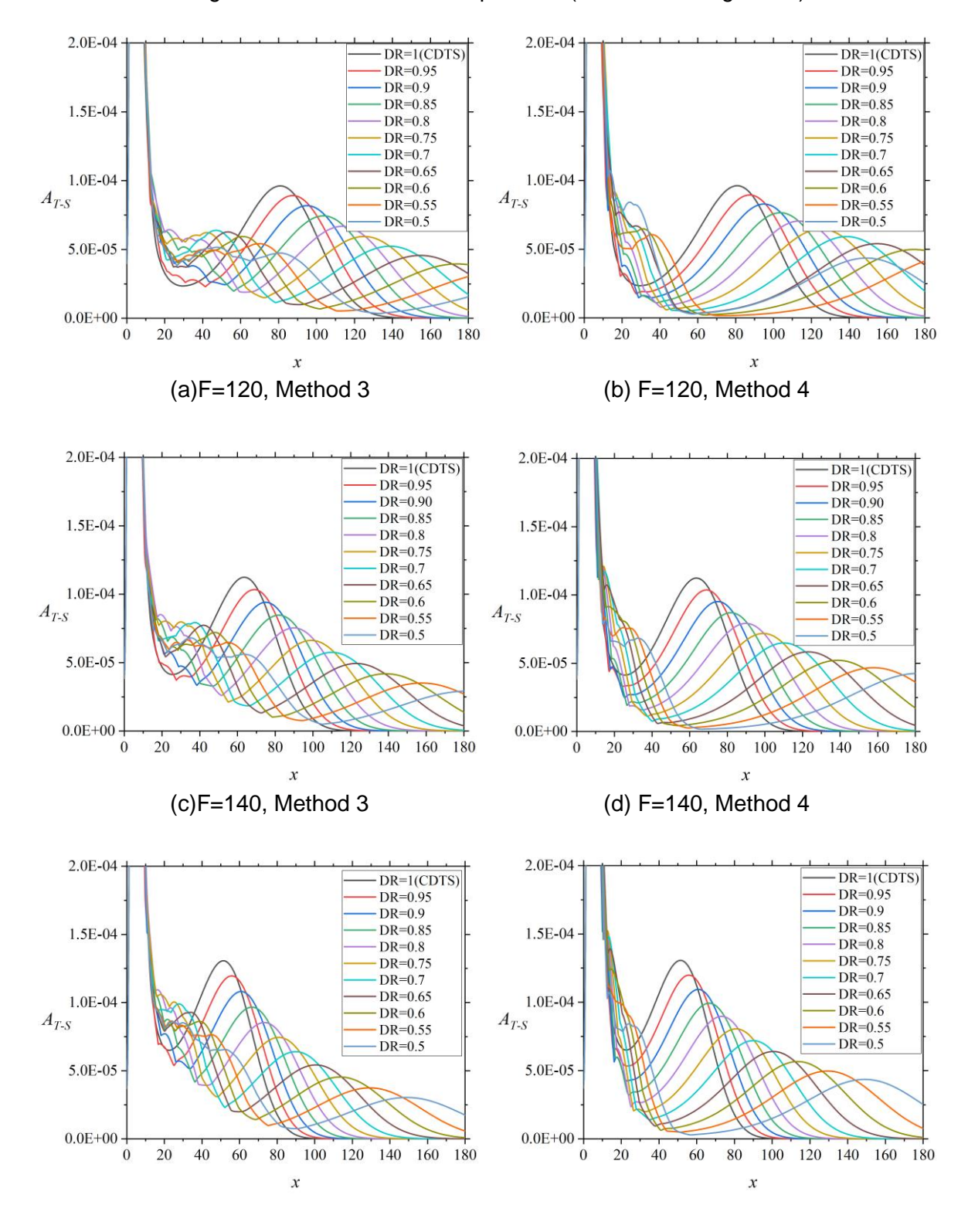
Considering that both Method 3 and 4 exhibit higher efficiency in terms of spectral analysis and the specific T-S waves excitement, the following discussion will focus on Methods 3 and 4.

4.4 The effect of duty ratio

This section explores the impact of the duty ratio on the amplitude, distribution, and frequency of the

excited T-S waves. Four frequencies were selected: F=120/140/160/180, and ten duty cycles (evenly distributed from 0.5 to 0.95). All of those are compared with the CDTS.

Figure 21 shows the distribution of the amplitude of the T-S waves excited by blowing and suction at different frequencies and duty ratios. It can be observed that as the duty ratio decreases, both the minimum and maximum points of the T-S wave amplitude gradually move downstream. The T-S waves excited by Method 3 have a smaller amplitude at the maximum point compared to those excited by Method 4. And the area around the minimum amplitude point is more chaotic, which may be related to Method 3 introducing disturbances of more frequencies (as shown in Figure 19).



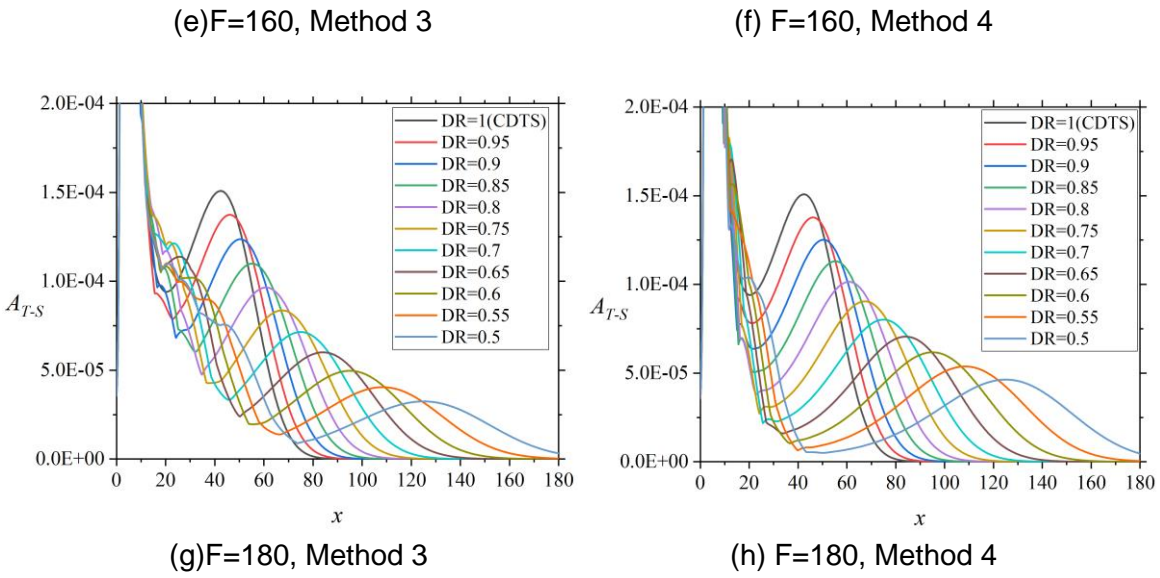
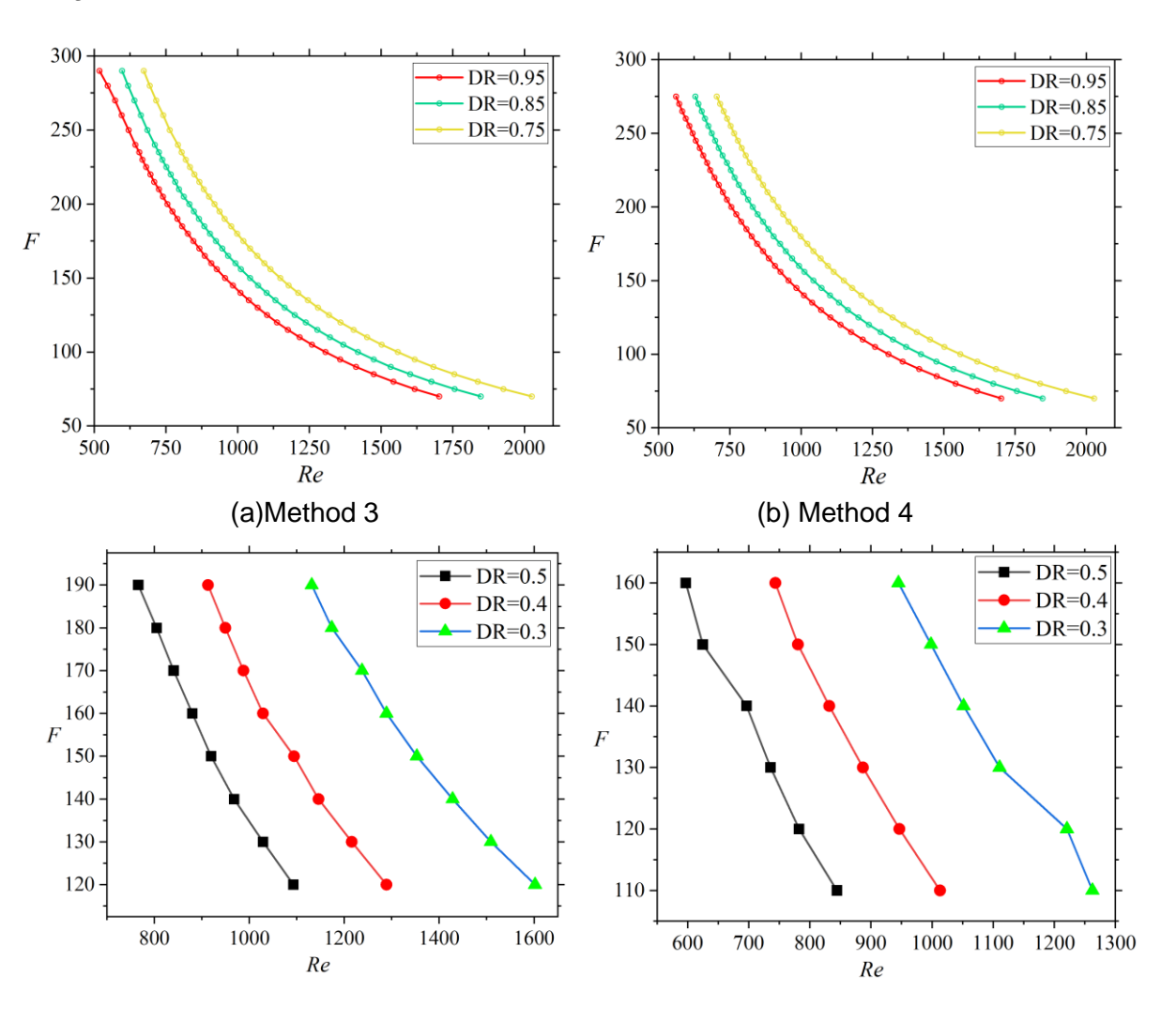


Figure 21 – Amplitude distribution of the T-S waves excited by different frequencies and duty ratios

Plot the Reynolds number of the second neutral point against the disturbance frequency and duty ratio in Figure 22. It can be observed that the trend of the curve is similar to the second branch of the neutral stability curve. However, as the duty ratio decreases, the curve shifts towards the upper right of the diagram.



(c)Method 3 (d) Method 4
Figure 22 – The "Nature Stability Curve" under different duty ratio

In the process of flow control involving T-S waves, the impact of frequency is also crucial. Artificially generating T-S waves with a stable frequency is fundamental to flow control. The next step in the research is to investigate the effect of duty ratio on frequency and the region of frequency stability. Figure 23 shows the spatial distribution of CDTS and T-S waves excited by duty ratios of 0.95, 0.85, and 0.75. The conclusion drawn in the figure first confirms part of the conclusions from Figure 21. For

and 0.75. The conclusion drawn in the figure first confirms part of the conclusions from Figure 21. For conditions with a low duty ratio, the T-S waves exhibit a smaller amplitude and a more disordered region upstream (for instance, when DR=0.75 and x<50), but gradually regain order as they propagate downstream. As the duty ratio decreases, the frequency of the orderly region of the T-S waves decreases, and their progression moves further downstream.

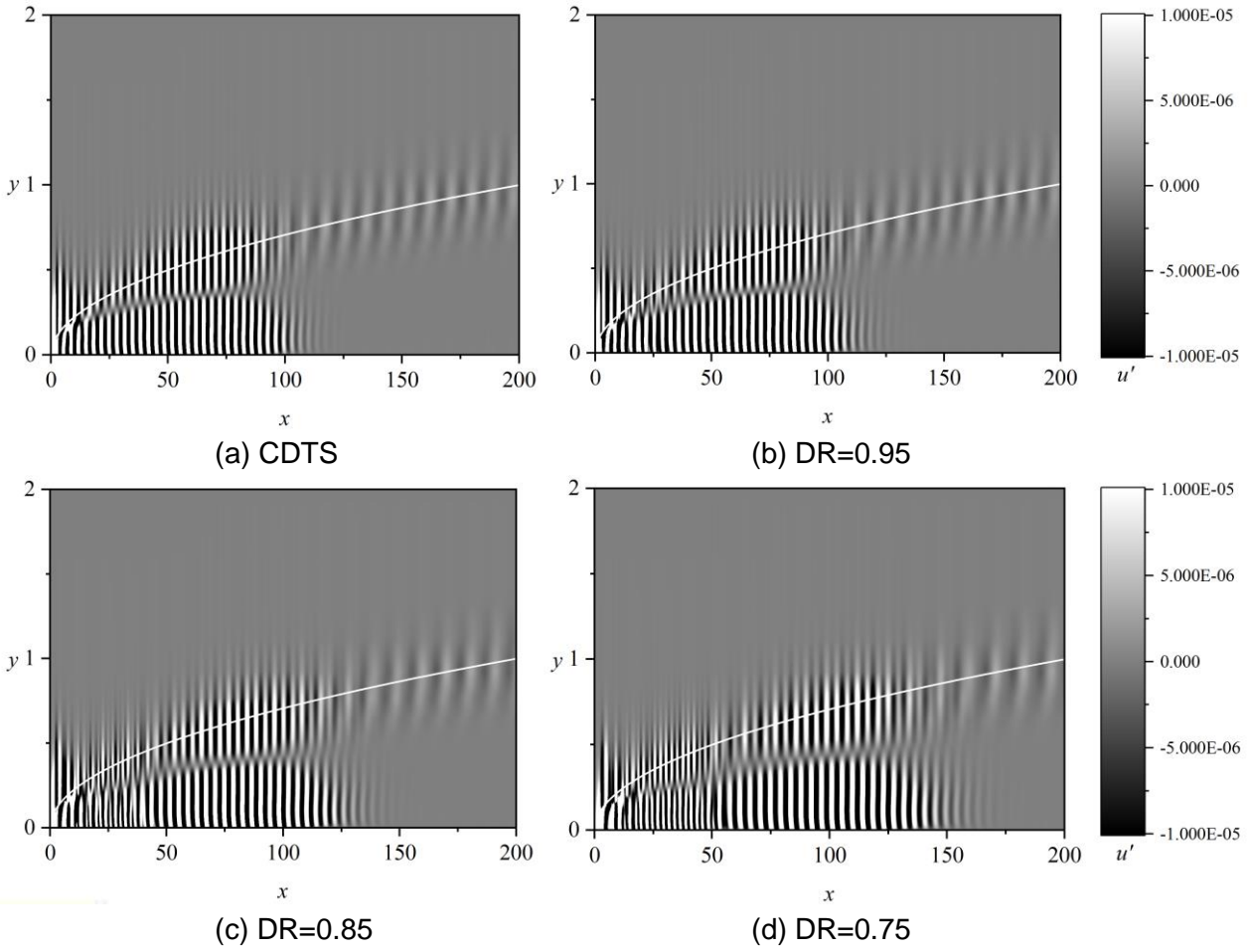


Figure 23 – Distribution of streamwise velocity fluctuation of T-S wave excited by different duty ratio

Further analysis of the frequency characteristics of the T-S waves is conducted. Figure 24 displays the contour lines where the fluctuation value of the T-S waves excited by the disturbance at F=140 and DR=0.95 is zero, along with frequency analysis of the T-S waves at two streamwise positions. It can be observed that the T-S waves excited by high-frequency disturbances have dissipated, and the frequency of the T-S waves at these locations is very stable.

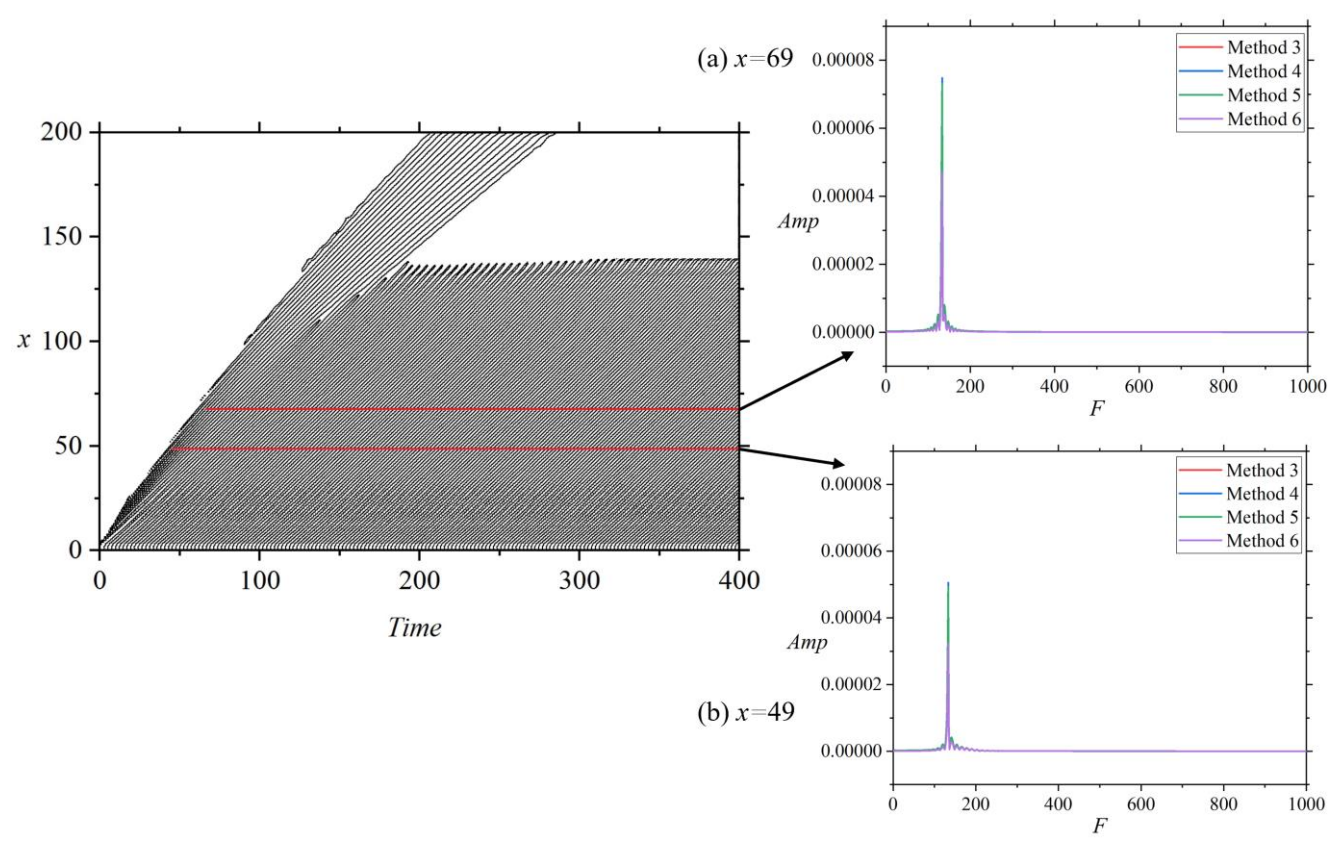


Figure 24 – Contour of velocity fluctuation u' = 0 and spectrum diagram

4.5 Efficiency analysis

Due to the characteristics of large amplitude and stable frequency of the T-S waves excited by intermittent blowing and suction, they can be utilized for the control of T-S waves, thereby suppressing transition to turbulence. Compared to traditional continuous disturbances that excite artificial T-S waves for flow control, intermittent blowing and suction can reduce the energy required for the disturbances, thus offering the advantage of low pump resistance. This section aims to analyze the efficiency of intermittent blowing and suction with the goal of controlling a set of CDTS at F=140. By examining the energy input required to achieve a controlled state and comparing it with traditional methods, the benefits of using intermittent disturbances can be quantified in terms of reduced energy consumption and lower pump drag, which is crucial for practical applications where energy efficiency and system performance are of concern.

In the research model of this paper, for the CDTS, the intersection of the second branch of the neutral stability curve with F=140 corresponds to a Reynolds number of 958.2, and the streamwise position x is 63.5. When the continuous disturbance amplitude is 1e-3, the amplitude of the CDTS at this neutral point (ABII) is 1.124e-4. Correspondingly, three intermittent blowing and suction conditions in method 4 are selected, as shown in Table 1.

 Amplitude
 Dimensionless frequency, F
 Duty Ratio, DR

 0.001
 147.37
 0.95

 0.001
 164.71
 0.85

 0.001
 186.67
 0.75

Table 1 Parameters for three cases of disturbance

The positions of the neutral stability points corresponding to the three conditions and the comparison of the T-S waves excited by the three conditions with the CDTS is presented in Figure 25. The specific amplitudes and efficiencies can be found in Table 2.

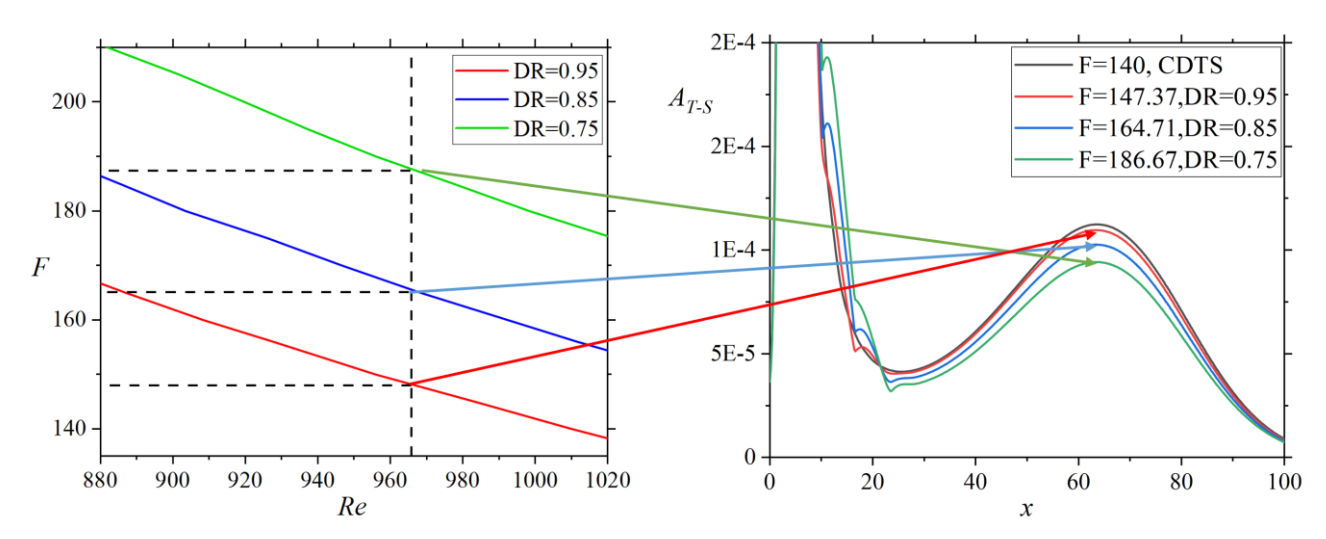


Figure 25 – Results of three conditions

Case	Amplitude of T-S wave, A_{T-S}	Energy saving
CDTS	1.124E-4	Baseline
F=147.37, DR=0.95	1.123E-4	5%
F=164.71, DR=0.85	1.026E-4	7%
F=186.67. DR=0.75	0.942E-4	12%

Table 2 Parameters for three cases of disturbance

It is found that when the same control effect is generated, the pump drag decreases with the decrease of duty ratio. When the blowing-suction duty ratio is 0.75, the maximum pump drag is reduced by more than 12%. However, it should be noticed that the duty ratio should not be less than 60 %, so as to avoid the adverse effect of low frequency disturbance on the boundary layer in the case of low duty ratio.

5. Conclusion

In this paper, direct numerical simulation (DNS) methods were employed, supplemented by wind tunnel experiments, to investigate the receptivity of laminar boundary layers to intermittent blowing and suction disturbances. The feasibility of using such disturbances as one of the means for hybrid laminar flow control (HLFC) was also assessed. The specific conclusions are as follows:

- 1. Basic Flow Analysis: The paper conducted an analysis of the basic flow, demonstrating that both the zero pressure gradient laminar boundary layer and the receptivity to continuous disturbances were in good agreement with linear stability theory. This validation confirms the reliability of the basic flow, providing a solid foundation for subsequent research.
- 2. Receptivity to Finite Periodic Disturbances: The study examined the characteristics of the initial wave, intermediate wave, and final wave, proposing the idea of utilizing these properties along with elementary waves for flow control.
- 3. Analysis of Elementary Waves: The paper conducted a frequency and other characteristic analyses of the T-S waves excited by a single-period sinusoidal disturbance, discovering that the frequency of the elementary waves continuously changes within the flow.

- 4. Proposal of Six Intermittent Blowing and Suction Methods: Two of the most efficient methods for exciting T-S waves (complete cycle blowing and suction + intermittent and complete blowing + intermittent + complete suction + intermittent) were identified. The study analyzed the receptivity to disturbances of different frequencies and duty ratios under these two methods, obtaining the corresponding neutral stability curves and spectra.
- 5. Efficiency Analysis of Intermittent Blowing and Suction: It was found that the blowing and suction Method 4 was the most efficient. Compared to the excitation of T-S waves using continuous disturbances, intermittent blowing and suction could improve efficiency by up to 12%, which is beneficial for reducing the pump drag in flow control.

6. Contact Author Email Address

The contact author: Zhen Cao, 2017caozhen@mail.nwpu.edu.cn.

7. Copyright Statement

The authors confirm that they, and/or their company or organization, hold copyright on all of the original material included in this paper. The authors also confirm that they have obtained permission, from the copyright holder of any third party material included in this paper, to publish it as part of their paper. The authors confirm that they give permission, or have obtained permission from the copyright holder of this paper, for the publication and distribution of this paper as part of the ICAS proceedings or as individual off-prints from the proceedings.

References

- [1] Wang X. A Review of NASA's First All-Electric X-plane, the X-57 Maxwell. *Electric propulsion*, No.2, pp 29-32, 2020.
- [2] Wang X. Sustainable Aviation Fuel Outlook. *Aerospace power*, No.2, pp 24-28, 2022.
- [3] International Air Transport Association. *Aircraft technology roadmap to 2050*. International Air Transport Association, 2020.
- [4] Deutsches Zentrum für Luft and Raumfahrt V. Development pathways for aviation up to 2050. German Aerospace Center, 2021.
- [5] Aerospace Technology Institute. FlyZero Aerodynamic structures technical report. Aerospace Technology Institute, 2022.
- [6] Aerospace Industries Association and Accenture. HORIZON 2050: A flight plan for the future of sustainable aviation. Aerospace Industries Association, 2022.
- [7] Collier F. An overview of recent subsonic laminar flow control flight experiments. 23rd Fluid Dynamics, Plasmadynamics, and Lasers Conference, Orlando, pp 2987, 1993.
- [8] Saric W, Reed H, White E. Stability and Transition of Three-Dimensional Boundary Layers. *Annual review of fluid mechanics*, 35, pp 413-440, 2003.
- [9] Schubauer G B, Harold S. Laminar-boundary-layer oscillations and transition on a flat plate. *Journal of research of the national bureau of standards*, Vol. 251, No.38, pp 327-357,1947.
- [10] Morkovin, Mark V. On the Many Faces of Transition. Viscous drag reduction, No.1, 1969.
- [11]Rogler H L, Reshotko Eli. Disturbances in a Boundary Layer Introduced by a Low Intensity Array of Vortices. *Siam journal on applied mathematics*, No. 28, pp 431-462, 1975.
- [12]Goldstein M E. The Evolution of Tollmien–Sclichting Waves near a Leading Edge. *Journal of fluid mechanics*. Vol.127, pp 59–81,1983.
- [13]Goldstein M E. Scattering of acoustic waves into Tollmien-Schlichting waves by small streamwise variations in surface geometry. *Journal of fluid mechanics*, Vol. 154, pp 509-529, 1985.
- [14] Crouch J D. Localized receptivity of boundary layers. *Physics of fluids A: fluid dynamics*, No.4, pp 1408-1414, 1992.
- [15] Choudhari M, Streett C L. A finite Reynold-number approach for the prediction of boundary-layer receptivity in localized regions. *Physics of fluids A: fluid dynamic*, No.4, pp 2495-2514,1992.
- [16]Bertolotti F P. Response of the Blasius boundary layer to free-stream vorticity. *Physics of fluids*, No. 9, pp 2286-2299, 1997.
- [17]Luo J, Zhou H. On the generation of Tollmien-Schlichting waves in the boundary layer of a flat plate by the disturbances in the free stream. *Mathematical and physical sciences*, Vol. 413, pp 351-367, 1987.
- [18]Deng X G. The application and development of CFD in large civil aircraft. Shanghai Jiao Tong University Press, 2009.
- [19]Robert W M. Tollmien–Schlichting wave cancellation. *Physics of fluids*, No.24, pp 979-981,1981.
- [20]Li Y, Gaster M. Active control of boundary-layer instabilities. *Journal of fluid mechanics*. Vol. 550, pp 185–205, 2006.
- [21]Sasaki K, Morra P, Fabbiane N et al. On the wave-cancelling nature of boundary layer flow control. *Theoretical and computational fluid dynamics*. Vol. 32, pp 593–616, 2018.
- [22]Simon B, Markus D, Tropea C et al. Cancellation of Tollmien–Schlichting Waves in Direct Vicinity of a Plasma Actuator. *AIAA Journal*, Vol. 56, No. 5, pp 1760-1769, 2018.
- [23]Brennan G S, Gajjar J S B, Hewitt R E. Tollmien–Schlichting wave cancellation via localised heating elements in boundary layers. *Journal of fluid mechanics*. Vol. 909, pp A16, 2021.
- [24]Zhu Z, Ju S, Wu Z. Laminar flow active/passive control technology. *Acta aeronauticaet astronautica sinica*, Vol. 37, No. 7, pp 2065-2090, 2016.
- [25]Green J. Laminar Flow Control Back to the Future? 38th Fluid Dynamics Conference and Exhibit. Seattle, pp 3738, 2008.
- [26] Fischer P F, Lottes J W, Kerkemeier S G. NEK5000 Web page, http://nek5000.mcs.anl.gov, 2008.
- [27] Saric W S, Reed H, Kerschen E. Leading-edge receptivity to sound-Experiments, DNS, theory. *AIAA Paper*, pp 2222, 1994.
- [28] Wang Z, Yeo K S, Khoo B C. On two-dimensional linear waves in Blasius boundary layer over viscoelastic layers. *European journal of mechanics-B/fluids*, Vol. 25, No. 1, pp 33-58. 2006.
- [29] Fasel H, Konzelmann U. Non-parallel stability of a flat-plate boundary layer using the complete Navier-Stokes equations. *Journal of fluid mechanics*, Vol.221, pp 311-347, 1990.
- [30]Hong Z, Ye Z. Numerical investigation of the evolution of two-dimensional T-S waves on an anisotropic compliant wall. *Chinese journal of theoretical and applied mechanics*, Vol.53, No.5, pp 1302-1312, 2021.